Available online at www.sciencedirect.com
ScienceDirect
Journal of the European Ceramic Society 30 (2010) 1833–1840
www.elsevier.com/locate/jeurceramsoc

Multilayer SiC for thermal protection system of space vehicles with decreased thermal conductivity through the thickness

S. Biamino [a,*], A. Antonini [a], C. Eisenmenger-Sittner [b], L. Fuso [c], M. Pavese [a], P. Fino [a], E. Bauer [b], C. Badini [a]

[a] *Dipartimento di Scienza dei Materiali e Ingegneria Chimica, Politecnico di Torino, Corso Duca degli Abruzzi 24, I-10129 Torino, Italy*
[b] *Institute of Solid State Physics, Vienna University of Technology, Wiedner Hauptstrasse 8-10, A-1040 Vienna, Austria*
[c] *Tecnogranda S.p.A., via G.B. Conte, 19, I-12025 Dronero (CN), Italy*

Received 10 March 2009; received in revised form 14 December 2009; accepted 22 January 2010
Available online 4 March 2010

Abstract

Tape casting combined with layer stacking, debinding and sintering proved to be a suitable technique for processing SiC-based multilayers to be used as thermal protection system for space vehicles. In this paper two methods have been evaluated in order to decrease the thermal conductivity through the thickness of the material: the insertion of layers containing a pore forming agent able to leave residual porosity; the deposition of an external insulating coating made of yttria-partially stabilized zirconia (YPSZ). Both techniques contribute to the reduction of thermal conductivity. The insertion into the multilayered structure of porous layers with a high level of residual porosity halves the thermal conductivity but 25% decrease in bending strength is observed. The fracture surface however shows that highly porous layers activates crack deflection mechanism, increasing fracture energy. The use of an YPSZ coating allows for a less evident reduction of thermal conductivity (from 102 to 75 W/(m K) at room temperature) but good mechanical properties are maintained (340 MPa bending strength).

Keywords: Tape casting; Mechanical properties; Thermal conductivity; SiC; Multilayer

1. Introduction

Thermal protection systems (TPS) represent a key issue for the successful re-entry of space vehicles and substantial improvements in the operational efficiency and reliability are needed, as well as cost reduction.[1]

At present, for this application, two different classes of materials have been considered: ultra high temperature ceramics (UHTC) such as ZrB_2/SiC or HfB_2/SiC composites.[2–6] and carbon fibre ceramic composites (in particular with SiC matrix).[7–9]

SiC shows potential for TPS, owing to its peculiar properties: thermal stability at very high temperature, low density, high stiffness and fairly good strength, high hardness and erosion resistance, self passivating behaviour in oxidising environment. However, SiC presents disadvantages that need to be overcome: rather poor toughness, poor thermal insulation capability at room temperature (even if greatly increasing with temperature increase[10]) and active oxidation at high temperature and under low oxygen partial pressure.[11,12]

Since Clegg showed that SiC-based multilayers can display improved toughness with respect to conventional monolithic SiC,[13,14] several multilayered ceramics have been widely investigated in the literature. In particular multilayered systems such as SiC/C,[13,15] SiC/SiC,[16] Al_2O_3/Al_2O_3,[17] Si_3N_4/BN,[18,19] Si_3N_4/Si_3N_4 whiskers,[20] ZrO_2 toughened Al_2O_3,[21,22] Al_2O_3/SiC[23] have been studied and found to exhibit higher fracture energy than their respective monolithic form. The key factor in multilayered ceramics is to provide the presence of weak interfacial bonds and/or controlled residual stresses between layers in order to increase the fracture energy thanks to crack deflection. The weak interfaces most commonly used are either graphite[13,15] or boron nitride.[18,19] However, since graphite and boron nitride have a low oxidation resistance and cannot be used at high temperature in oxidising atmosphere without a protective barrier, other systems have been investigated. As a necessary condition for the interfacial material

* Corresponding author. Tel.: +39 011 5644674; fax: +39 011 5644699.
E-mail address: sara.biamino@polito.it (S. Biamino).

0955-2219/$ – see front matter © 2010 Elsevier Ltd. All rights reserved.
doi:10.1016/j.jeurceramsoc.2010.01.040

Table 1
Composition of the three kinds of slurries and dry green tapes.

Component	Fully densifying		20%porous		60%porous	
	Slurry (wt.%)	Dry tape (wt.%)	Slurry (wt.%)	Dry tape (wt.%)	Slurry (wt.%)	Dry tape (wt.%)
SiC	33.6	67.7	27.9	58.7	15.2	35.2
B	0.3	0.6	0.3	0.6	0.2	0.5
C	1.0	2.0	0.8	1.7	0.5	1.2
Pore forming agent	–	–	3.3	6.9	10.6	24.5
Solvents	50.4	–	52.4	–	56.8	–
Dispersant	0.1	0.2	0.1	0.2	0.1	0.2
Binder	9.6	19.4	10.0	21.0	10.9	25.2
Plasticiser	5.0	10.1	5.2	10.9	5.7	13.2

is that it must be chemically compatible with the material of the strong layers, ceramic laminates with alternating dense and porous layers have been studied.[16,17,20,24–26]

Several processing methods can be used to fabricate multilayered structures such as extrusion[23] or electrophoretic deposition[15] but the most used method is tape casting followed by debinding and sintering.[16,17,21,22,27–33]

Despite the great attention dedicated in the literature to the preparation processing[24] and mechanical behaviour[16,25,26] of multilayer structures alternating dense and porous layers prepared by tape casting there is a lack of investigation about the consequent variation of their thermal properties.

In a previous paper,[34] we already proposed SiC-based laminate containing porous layers (prepared by tape casting, debinding and sintering) as a promising material to be employed for TPS of space vehicles and we described the behaviour of this material when submitted to thermal re-entry tests under test conditions representing the trajectory of the HERMES vehicle.[35]

Owing to the promising thermal performance of this material, the presence of porous layers in the architecture of SiC-based laminates was further investigated in this paper. As an alternative was also studied the possibility of reducing conductivity by spraying on the surface an yttria-partially stabilized zirconia (YPSZ) coating, which is the current state-of-the-art material for thermal barrier coatings.[36,37] Planar characteristics of the multilayers are expected not to be altered by in-thickness structure modifications. Preparation of the samples, together with their mechanical and thermal behaviour was investigated, as a function of the number and porosity of porous layers, as well as the presence of the YPSZ coating.

2. Experimental

Multilayered SiC specimens were prepared, based on our previous investigations, with tape casting technology.[33,34,38,39] The processing method involved several steps: slurry preparation, tape casting, solvent evaporation, layer stacking, debinding and sintering. The slurry was obtained by dispersing SiC powder (grade UF 15 produced by Starck, particle size 0.55 μm and specific surface area 14–16 m^2/g), with boron powder (grade I produced by Starck, particle size 1–2 μm and specific surface area >10 m^2/g) and graphite powder (flake 7–10 μm produced by Alfa Aesar) as sintering aids, together with dispersant (fish oil) in a mixture of organic solvents (ethanol, butanol and tetrachloroethylene in approximate weight percent rates of 23, 36 and 41). After ball milling for about 24 h, plasticiser (polyethylene glycol) and binder (polyvinyl butyral) were added; ball milling was then continued for about 24 h. Al_2O_3 jars were used, with Al_2O_3 milling balls. This kind of slurry and the derived tapes are labelled as "fully densifying".

Since the aim of this work was to investigate the effect of the presence of porous layers in the multilayered structure of the specimens, two other slurries containing a pore forming agent (starch, by Sigma–Aldrich) were prepared. In one case 20 vol% of SiC powder was replaced by an equal volume of starch and in the other case 60 vol% of SiC powder was substituted by an equal volume of starch. These slurries and their derived tapes are labelled as "20%porous" and "60%porous", respectively. All the slurries are detailed in Table 1.

Thin sheets were produced by casting the slurries on a moving Mylar support and the layer thickness was controlled by selecting the blade gap (1 mm) and the casting velocity (100 mm/min). The as cast slurry was left to dry on the flat surface of the tape casting apparatus for about 12 h, thus allowing the organic solvents to be completely removed by slow and controlled evaporation in air.

After drying, all the tapes were easily detached from the plastic support (showing high flexibility) and were characterized in term of thickness and roughness (Table 2). The roughness of the green tapes was measured by MAHR Perthometer M1. The two sides of the tapes (the one in contact with the Mylar film and the one in contact with the open air) showed different surface roughness, the side in contact with the Mylar film being the smoother one. In addition an increase of roughness can be observed with the increase of starch content in the slurry; this is particularly

Table 2
Thickness and roughness of the three kinds of dry green tapes.

Kind of tape	Thickness (mm)	Roughness (μm)	
		Open air side	Mylar side
Fully densifying	0.25	0.3–0.4	0.1–0.2
20%porous	0.24	0.7–0.8	0.1–0.2
60%porous	0.22	1.6–1.9	0.2–0.3

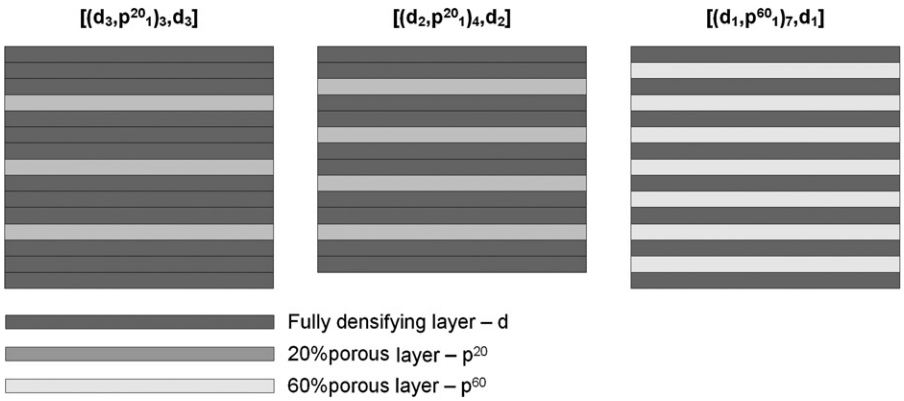

Fig. 1. Schematic examples of some multilayer architecture prepared (coupled to their respective nomenclature).

evident for the open air side. In Table 1 the composition of the dry green tapes is given.

After detachment, the green tapes were cut to the desired final shape and stacked one upon the other to form the multilayered specimens. In particular several architectures were prepared by alternating in different ways the three types of layers: "fully densifying" and "20%porous" or "60%porous". To describe the sequence of the layers which constitutes a sample, a standard method is used. For example the expression $[(d_2,p^{20}{}_1)_4,d_2]$ means a sample made of 14 layers stacked in the following sequence: two "fully densifying" layers and one "20%porous" layer, these repeated four times, and two "fully densifying" layers again. In Fig. 1 some examples of the architectures used are depicted.

The adhesion between the layers was attained by painting a gluing solution made of water, ethanol and polyvinyl alcohol (PVA) before stacking, and then rolling with a mandrel in order to let the next layer adhere without the formation of air bubbles. Attention was paid to attach a rough surface to a smooth one for the adhesion benefit.

The specimens were then submitted to a debinding treatment, carried out by slow heating up to 800 °C under an argon atmosphere in order to prevent SiC oxidation. The heat treatment was optimized by previous investigations of the decomposition of the organic components of the green tape, performed by making use of thermogravimetric analysis (TGA/SDTA Mettler-Toledo). The starch acts as a pore forming agent because during the debinding treatment it undergoes decomposition, thus giving a residual porosity which is not completely recovered during the subsequent sintering.

The final pressureless sintering step was performed in a graphite furnace (TAV TS 150/250 CRISTALOX) at a temperature in the range 2100–2300 °C under 600 mbar argon atmosphere for 30 min.

Some promising architectures were chosen in order to evaluate the effectiveness of an external insulating coating of 3 mol.% yttria-partially stabilized zirconia deposited by spray solution combustion synthesis.[40,41] An aqueous solution containing the metal precursors of YPSZ (zirconyl nitrate hydrate, $ZrO(NO_3)_2$ from Sigma–Aldrich and yttrium nitrate, $Y(NO_3)_3$ from Sigma–Aldrich) and a sacrificial fuel (urea, $CO(NH_2)_2$ from Sigma–Aldrich) was prepared according the stoichiometry of reactions (1) and (2).

$$3ZrO(NO_3)_2 + 5CO(NH_2)_2 \rightarrow 3ZrO_2 + 5CO_2 + 8N_2 + 10H_2O \quad (1)$$

$$2Y(NO_3)_3 + 5CO(NH_2)_2 \rightarrow Y_2O_3 + 5CO_2 + 8N_2 + 10H_2O \quad (2)$$

After a few minutes of stirring on a heating plate to ensure proper homogeneity, the solution was transferred with an airbrush and sprayed on the sample, which had been preheated at 600 °C and which was immediately inserted again into the oven where reactions (1) and (2) took place. After a few minutes the reaction was over, resulting in an oxide layer on the support. The specimen was then removed from the oven, let to cool and blown with compressed air in order to remove the material not properly adherent to the specimen surface. The whole process (sample preheating, solution spraying, reaction into oven, sample cooling and air blowing) was repeated a number of times in order to reach a proper thickness of the YPSZ layer on the specimen (15 repetitions are affective for the deposition of a 60 μm coating).

In order to verify the adhesion of the oxide layer to the support, samples were stressed in an ultrasonic bath (180 W) for different periods and weighed.

The density of the coated and uncoated samples was measured both geometrically and using Archimedes' principle in water, in order to distinguish between total porosity and porosity accessible by the extern. Three-point bending tests were performed on uncoated samples according to UNI EN 658.3 standard (Sintech 10D equipment) with a crosshead speed of 0.1 mm/min and a span of 40 mm. The deflection occurring during the test is perpendicular to the layers and the length of the sample is parallel to the casting direction. Rectangular samples were used to measure Young's modulus according to ASTM C 1259-01 by using an impulse excitation technique involving the analysis of the transient composite natural vibration (GrindoSonic MK5 instrument). Microhardness was measured making use of Vickers indentation with a load of 500 g and for a dwelling time of 10 s.

Fig. 2. Examples of X-ray radiographies performed on sintered samples as non-destructive test.

Thermal diffusivity was measured using a commercial thermal flash system (Anter Flashline 3000) equipped with a high temperature stage which allows thermal diffusivity measurements from RT to 1000 °C. The thermal flash technique has been pioneered by Parker et al.[42] This instrument employs a high-speed xenon flash lamp to illuminate the front of the sample and records the corresponding rise in the backside temperature with an infrared detector. The flash technique allows the sample heat capacity determination too by alternately measuring a reference and the sample. So thermal conductivity can be evaluated when the sample density is known and separately entered into the instrument software.

All testing is performed on at least five samples, in order to improve the statistical significance of the results. A non-destructive test (X-ray radiography) was performed on the sintered specimens before the thermo-mechanical characterization in order to exclude the presence of macroscopic defects; examples are reported in Fig. 2.

The microstructure and chemical composition of the samples were assessed by Scanning Electron Microscopy (SEM-FEG Assing SUPRA 25) coupled with Energy Dispersive Spectroscopy (EDS Oxford), traditional X-ray diffraction (Philips PW1710 CuK_{α} radiation) and X-ray microdiffraction (Rigaku D/MAX Rapid, spot size down to 10 μm diameter).

3. Result and discussion

Debinding is a fundamental step for the preparation of multilayer ceramics, since it consists in the softening of the binder followed by the decomposition of organics (binder and plasticiser), resulting in the evolution of gaseous species.[43]

In order to study the debinding of the organic compounds present in the ceramic slurry, thermogravimetric analysis were performed (see Fig. 3) on fully densifying (curve A), 20%porous (curve B) and 60%porous (curve C) green multilayer samples. The decomposition of organics species occurred mainly between 200 and 500 °C. However, with the increase of the amount of starch, both the total weight loss increases and the initial decomposition temperature decreases, starting at about 100 °C. The optimized debinding treatment was chosen in order to avoid fast gas evolution during the organics decomposition, and satisfying results were obtained using the following procedure:

- a slow heating rate of 0.1 °C/min from ambient temperature up to 500 °C; this is the critical step of the process, since the main gaseous evolution occurred between 100 and 500 °C;

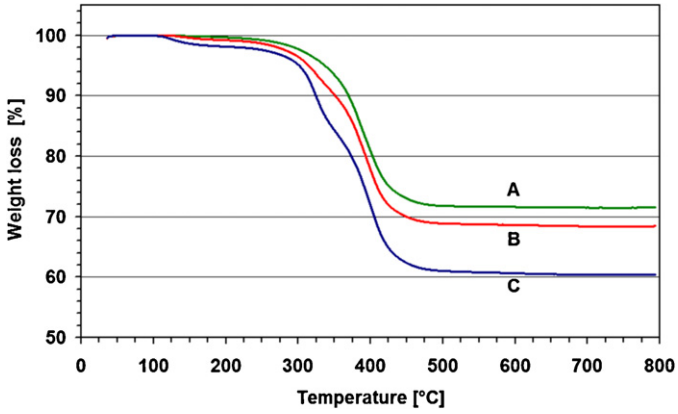

Fig. 3. Thermogravimetric analysis: (A) $[d_{15}]$, (B) $[(d_1,p^{20}{}_1)_7,d_1]$ and (C) $[(d_1,p^{60}{}_1)_7,d_1]$.

- a more rapid heating rate of 0.5 °C/min up to 800 °C followed by an isotherm of 30 min in order to assure the completion of the process.

The whole treatment was done under argon flow in order to prevent undesired oxidation of SiC particles.

In Fig. 4 the fracture surface of a debinded sample is depicted. It can be noted that after debinding the specimens consist of compacted powder only. This emphasizes the intrinsic brittleness of the debinded samples and the need to control the gaseous evolution during the heat treatment, in order to avoid disturbing the powder structure. A mean shrinkage of about 3% occurred during debinding.

A certain amount of carbonaceous residues remains in the debinded specimen (about 6 wt.% left by binder and 3 wt.% left by plasticiser). According to these outcomes and knowing the composition of dry tapes (Table 1), we can estimate that about 2 wt.% of residual carbonaceous species remains after the debinding process. Together with the graphite expressly forming

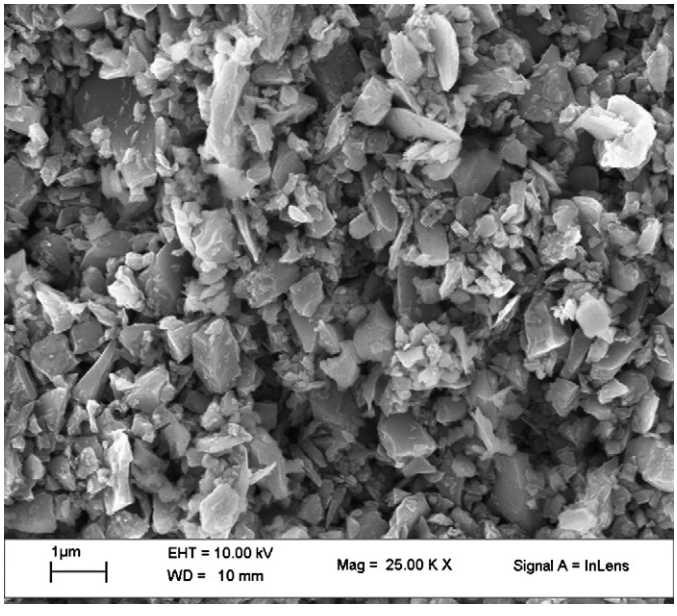

Fig. 4. SEM microstructures of fracture surfaces for a sample after debinding.

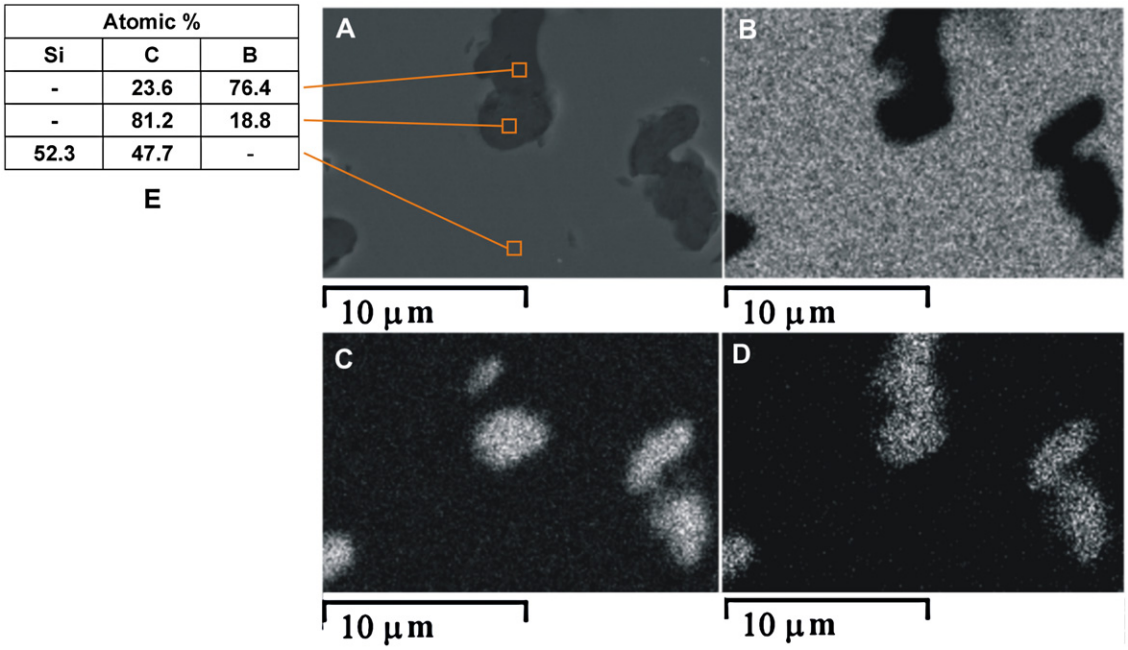

Fig. 5. SEM–EDS analysis on a polished surface (sample sintered at 2200 °C): (A) SEM image, (B) elemental map for silicon, (C) elemental map for carbon, (D) elemental map for boron and (E) EDS analysis of the different zones.

part of the mix, it results in a total 4.8 wt.% of carbon. According to the literature[44] the optimum amount of carbon as SiC sintering aid in presence of boron is in the range 3–6 wt.%.

The optimal sintering temperature was found to be 2200 °C, because higher temperatures resulted in grain growth without a significant density improvement (grain size at 2200 °C was 4–9 μm and at 2300 °C was 12–23 μm). The mean cumulative shrinkage after both debinding and sintering is about 20%.

The microstructures of all the sintered samples mainly consist of three phases, as shown by SEM coupled with element maps and with EDS analysis (Fig. 5): the main grey area was SiC, while two kinds of dark grey zones were observed and contained carbon and boron in different amounts: the more frequent richer in carbon, the rare one richer in boron. This was confirmed by X-ray diffraction and microdiffraction, where only SiC and carbon were detected, thus indicating that boron rich zones are less frequent.

Microhardness measurements conducted separately on fully densified layers and on 60%porous layers gave a result of about 2300–2500 and 1100–1400 HV, respectively.

The overall density of a specimen is affected by the insertion of the porous layers as shown in Fig. 6, where the average density for different types of specimen is given both in terms of geometric density and Archimedes' density in order to distinguish between total porosity and open porosity. The difference between Archimedes' density and the geometric one is of the same degree for all specimens, with a slightly greater difference for the specimens containing "60%porous" layers thus suggesting a slight increase in porosity accessible by the extern in these cases.

The classification of the samples in terms of density clarified the results of the thermal diffusivity/conductivity tests and, to some extent, of the mechanical tests. In general it is possible to

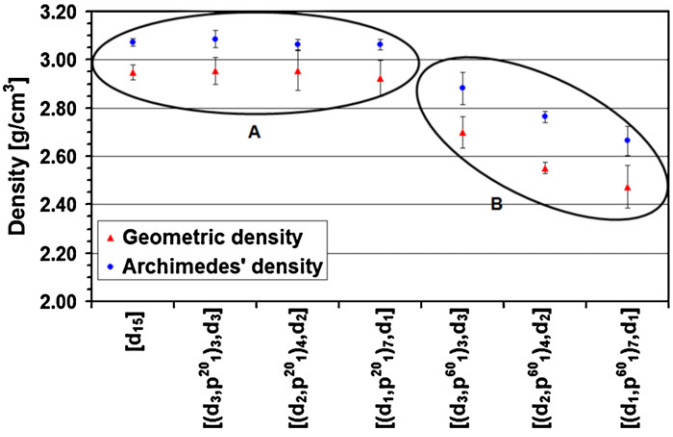

Fig. 6. Geometric density and Archimedes' density depending on sample architecture.

observe that the integration in the architecture of "20%porous" layers does not change the overall density from that of specimens made of fully densifying layers only (see circle A in Fig. 6). In contrast, the integration in the architecture of "60%porous" layers effectively resulted in a decrease of the overall specimen density (see circle B in Fig. 6). The higher the number of porous layers the greater the reduction of density.

Table 3
Three-point bending strength and Young's modulus of three kinds of specimens.

Sample	Flexural strength (MPa)	Young modulus (GPa)
$[d_{11}]$	342	360
$[(d_3,p^{20}{}_1)_2,d_3]$	336	370
$[(d_3,p^{60}{}_1)_2,d_3]$	250	283

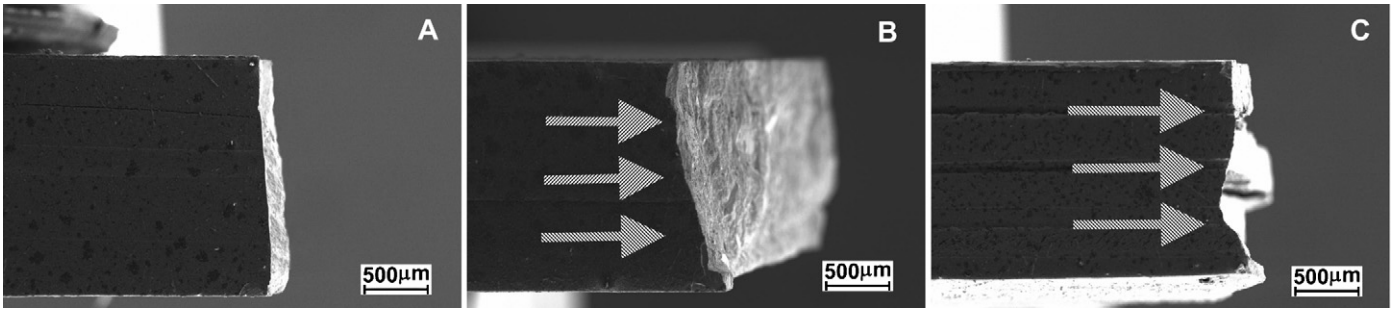

Fig. 7. SEM images of fracture surfaces (macroscopic view of the sample side): (A) [d_{11}], (B) [$(d_2,p^{20}{}_1)_3,d_2$] and (C) [$(d_2,p^{60}{}_1)_3,d_2$].

In Table 3 are reported the results of three-point bending tests and of Young's modulus measurements for the three kinds of specimen. Both mechanical strength and elastic modulus are significantly affected by the presence of the "60%porous" layers into the architecture, with a reduction of about 25% of the measured values with respect to the fully densifying samples. The "20%porous" samples presented very similar values to the fully densifying ones.

In Fig. 7 the fracture surfaces of the specimens after the 3-point bending test are shown, confirming that the "60%porous" layer acts as a weaker link which activates a deflection of the approaching cracks thus increasing the fracture surface energy.

Particularly interesting were the results of thermal diffusivity measurements (Fig. 8). In fact, as with density, the "20%porous" layers do not drastically change the diffusivity from that of the specimen made of fully densifying layers only (group A in Fig. 8): 0.53 cm^2/s at room temperature and 0.15 cm^2/s at 900 °C. In contrast, the integration in the architecture of "60%porous" layers resulted in halving the diffusivity through the thickness of the material (group B in Fig. 8): from 0.53 cm^2/s down to 0.27 cm^2/s at room temperature and from 0.15 cm^2/s down to 0.08 cm^2/s at 900 °C.

Since the measured value is the thermal diffusivity, only this value is reported in the graph. Thermal conductivity can be calculated from thermal diffusivity by measuring the specific heat of the samples. The corresponding mean calculated thermal conductivity values for the two groups were 102 W/(m K) at room temperature and 45 W/(m K) at 900 °C for group A as well as 42 W/(m K) at room temperature and 23 W/(m K) at 900 °C for group B.

In Fig. 9 a selection of diffusivity measurements performed on specimens coated with the external YPSZ layer are shown and compared with the average values of groups A and B above mentioned (see dotted lines). In particular, for the evaluation of the effectiveness of the YPSZ layer, specimen architectures belonging to group A (sample [$(d_3,p^{20}{}_1)_3,d_3$]) and to group B (sample [$(d_3,p^{60}{}_1)_3,d_3$]) have been selected. Furthermore on sample [$(d_3,p^{20}{}_1)_3,d_3$] the effect of the thickness of the YPSZ coating has been investigated. It can be seen that a 60 µm YPSZ coating is effective in reducing the thermal diffusivity through the thickness only for those specimens which are made of all "fully densifying" layers or which contain "20%porous" layers (group A samples): from 0.53 to 0.41 cm^2/s at room temperature and from 0.15 to 0.12 cm^2/g at 900 °C. The consequent mean calculated thermal conductivity values at room temperatures were: 102 W/(m K) for uncoated specimens and 75 W/(m K) for coated ones.

The increase in coating thickness from 60 to 90 µm had a visible effect only at low temperature where a further reducing thermal diffusivity to 0.35 cm^2/s is observed. The coating deposited on multilayers containing "60%porous" layers, on the contrary, do not show a reduction of thermal diffusivity values, but a small increase is observed. Thermal diffusivity passes from 0.27 to 0.31 cm^2/s at room temperature, while at 900 °C

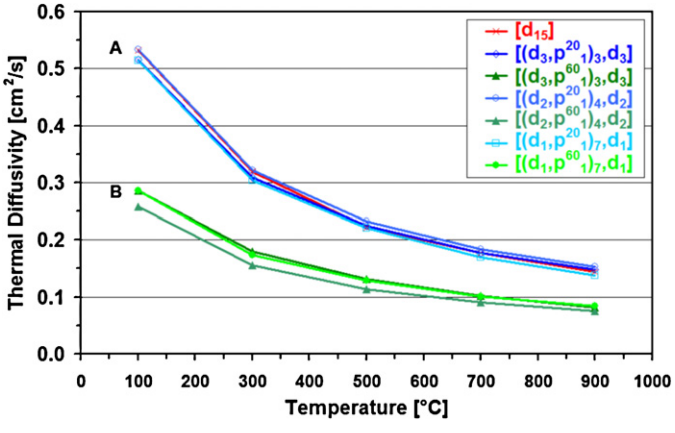

Fig. 8. Thermal diffusivity measurements versus temperature depending on sample architecture.

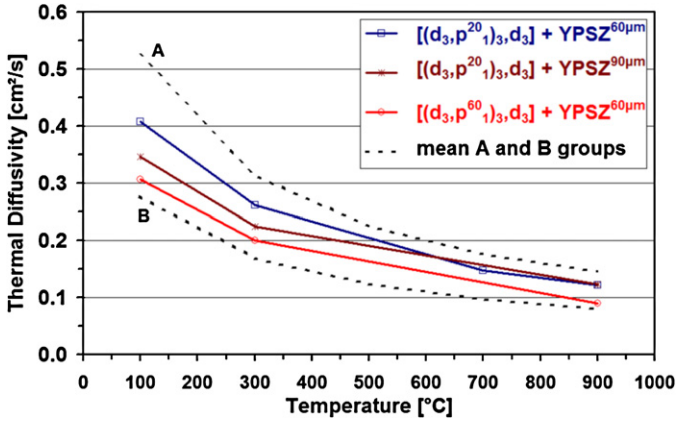

Fig. 9. Influence of the external insulating YPSZ coating on thermal diffusivity measurements versus temperature depending on the sample architecture and comparison with uncoated samples (dotted curves A and B).

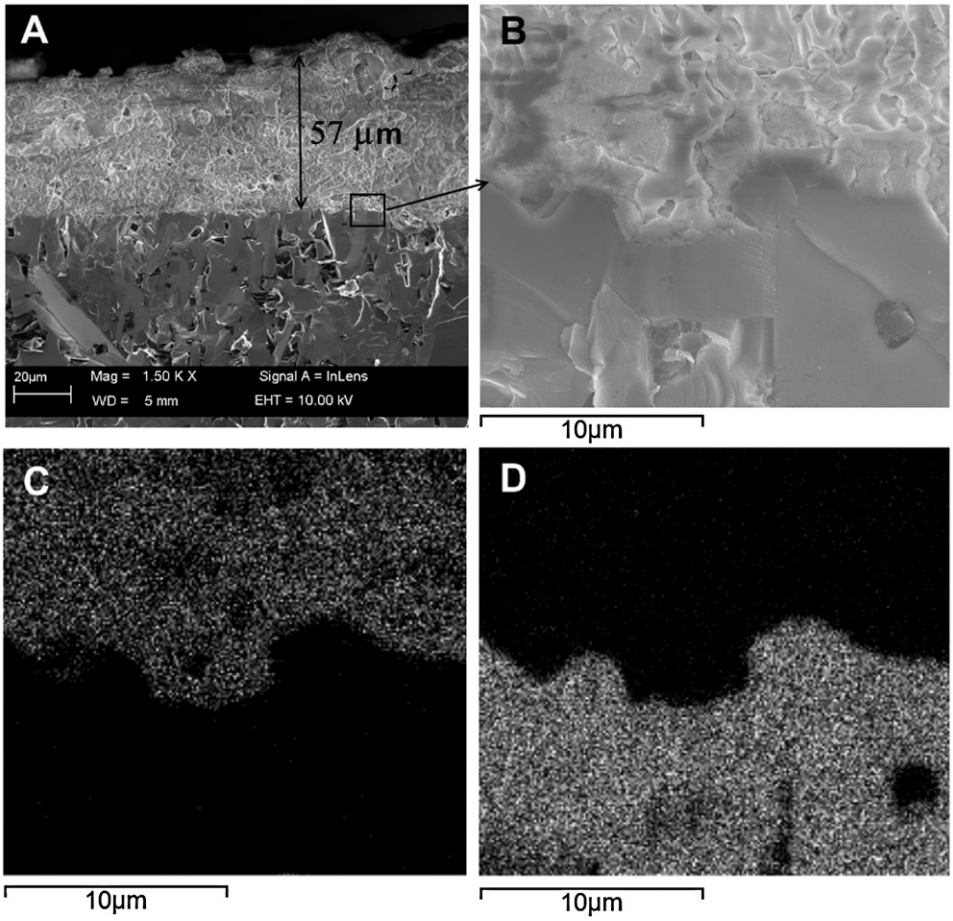

Fig. 10. SEM–EDS analysis on a coated sample: (A) SEM image showing the coating thickness, (B) detail of the interface between the YPSZ coating and the SiC substrate, (C) elemental map for zircon and (D) elemental map for silicon.

the difference is very small, suggesting that the effect of the porous layers in this case is stronger than the effect of the YPSZ coating.

The adhesion tests proved that the adherence between the deposited YPSZ and the SiC support is excellent; in fact the oxide is strongly bonded to the support and even high intensity and lengthy vibrations in the ultrasonic bath cannot damage the system. In Table 4 the average values of weight loss versus the duration of sample treatment in an ultrasonic bath are reported. It must be specified that weight percentages were calculated referring to the weight of deposited oxide only. After a first weight loss of about 5% the samples do not have further significant variations. In Fig. 10A a SEM micrograph showing the external YPSZ layer is reported. In particular the repetition of the deposition process for 15 times was effective for the formation of about 60 μm YPSZ layer. In Fig. 10B a detail of the interface zone, coupled to the elemental maps for Zr and Si (Fig. 10C and D, respectively), shows the solid interface between SiC and YPSZ.

Table 4
Average weight loss of YPSZ coating after different time in ultrasonic bath.

Time (min)	Cumulative weight loss (%)
15	4.88
30	5.38
60	5.54

4. Conclusion

In this paper two methods have been evaluated and combined in order to decrease the thermal conductivity through the thickness of SiC multilayers.

The first way is to insert layers containing a pore forming agent able to give a residual porosity after sintering. The second way is to deposit an external insulation coating made of yttria-partially stabilized zirconia (YPSZ) by means of spray combustion synthesis.

The presence of porous layers in the architecture of the specimen can be effective to decrease the thermal diffusivity. By inserting highly porous layers in the multilayer it has been possible to halve the thermal diffusivity through the thickness, that goes from 0.53 to 0.27 cm^2/s at room temperature and from 0.15 to 0.08 cm^2/s at 900 °C. The presence of highly porous layers however degrades the mechanical properties, with the flexural strength going from 342 to 250 MPa for a sample with halved thermal conductivity, even if allow the triggering of crack deflection mechanisms.

Differently, the deposition of an external insulating coating allows to decrease the thermal diffusivity through thickness

mainly for dense or slightly porous layers. The decrease in this case is less marked, going from 0.53 to 0.41 cm^2/s at room temperature and from 0.15 to 0.12 cm^2/s at 900 °C; however in this cases, no significant variation in mechanical properties is observed.

Acknowledgements

This work has been performed within the framework of the Integrated European Project "ExtreMat" (contract NMP-CT-2004-500253) with financial support of the European Community. It only reflects the view of the authors and the European Community is not liable for any use of the information contained therein.

References

1. Behrens B, Muller M. Technologies for thermal protection systems applied on re-usable launcher. *Acta Astronaut* 2004;**55**:529–36.
2. Scatteia L, Borrelli R, Marino G, Bellosi A, Monteverde F.*A collection of technical papers. 13th AIAA/CIRA international space planes and hypersonic systems and technologies conference*. American Institute of Aeronautics and Astronautics; 2005. p. 613.
3. Han J, Hu P, Zhang X, Meng S, Han W. Oxidation-resistant ZrB_2–SiC composites at 2200 °C. *Comp Sci Technol* 2008;**68**:799–806.
4. Levine SR, Opila EJ, Halbig MC, Kiser JD, Singh M, Salem JA. Evaluation of ultra-high temperature ceramics for aeropropulsion use. *J Eur Ceram Soc* 2002;**22**:2757–67.
5. Savino R, De Stefano Fumo M, Paterna D, Serpico M. Aerothermodynamic study of UHTC-based thermal protection systems. *Aerospace Sci Technol* 2005;**9**:151–60.
6. Monteverde F, Bellosi A, Scatteia L. Processing and properties of ultra-high temperature ceramics for space applications. *Mater Sci Eng A* 2008;**485**:415–21.
7. Pichon T, Soyris P, Foucault A, Parenteau JM, Prel Y, Guedron S. C/SiC based rigid external thermal protection system for future reusable launch vehicles: generic shingle, pre-X/FLPP anticipated development test studies. In: *Proceedings of the 5th European workshop on "Thermal Protection Systems and Hot Structures"*. Noordwijk (The Netherlands): ESA-ESTEC; 2006., ISBN 92-9092-942-1.
8. Liedtke V, Huertas Olivares I, Langer M, Haruvy YF. Manufacturing and performance testing of sol/gel based oxidation protection systems for re-usable space vehicles. *J Eur Ceram Soc* 2007;**27**:1493–502.
9. Mue Hlratzer A, Handrick K, Pfeiffer H. Development of a new cost-effective ceramic composite for re-entry heat shield applications. *Acta Astronaut* 1998;**42/9**:533–40.
10. Munro RG. Material properties of a sintered α-SiC. *J Phys Chem Ref Data* 1997;**26**(5):1195–203.
11. Gulbransen EA, Jansson SA. The high-temperature oxidation, reduction, and volatilization reactions of silicon and silicon carbide. *Oxid Metals* 1972;**4**(2):181–201.
12. Jacobson NS, Fox DS, Opila EJ. High temperature oxidation of ceramic matrix composites. *Pure Appl Chem* 1998;**70**(2):493–500.
13. Clegg WJ. A simple way to make tough ceramics. *Nature* 1990;**347**:455–7.
14. Clegg WJ. The fabrication and failure of laminar ceramic composites. *Acta Metall Mater* 1992;**40**(11):3085–93.
15. Vandeperre L, Van Der Biest O. Composite SiC-graphite interlayers for crack deflection in ceramic laminates. *Silic Ind* 1998;**63**:39–43.
16. Blanks KS, Kristoffersson A, Carlström E, Clegg WJ. Crack deflection in ceramic laminates using porous interlayers. *J Eur Ceram Soc* 1998;**18**:1945–51.
17. Davis JB, Kristoffersson A, Carlström E, Clegg WJ. Fabrication and crack deflection in ceramic laminates with porous interlayers. *J Am Ceram Soc* 2000;**83**:2369–74.
18. Liu H, Hsu SM. Fracture behaviour of multilayer silicon nitride/boron nitride ceramics. *J Am Ceram Soc* 1996;**79**:2452–7.
19. Kovar D, Thouless MD, Halloran JW. Crack deflection and propagation in layered silicon nitride/boron nitride ceramics. *J Am Ceram Soc* 1998;**81**:1004–12.
20. Ohji T, Shigegaki Y, Miyajima T, Kanzaki S. Fracture resistance behaviour of multilayered silicon nitride. *J Am Ceram Soc* 1997;**80**:991–4.
21. Chartier T, Merle D, Besson JL. Laminar ceramic composites. *J Eur Ceram Soc* 1995;**15**:101–7.
22. Chartier T, Rouxel T. Tape cast alumina–zirconia laminates: processing and mechanical properties. *J Eur Ceram Soc* 1997;**17**:299–308.
23. She J, Inoue T, Kazuo U. Multilayer Al_2O_3/SiC ceramics with improved mechanical behaviour. *J Eur Ceram Soc* 2000;**20**:1771–5.
24. Reynaud C, Thevenot F, Chartier T. Processing and microstructure of SiC laminar composites. *Int J Refract Metals Hard Mater* 2001;**19**:425–35.
25. Ma J, Wang H, Weng L, Tan GEB. Effect of porous interlayers on crack deflection in ceramic laminates. *J Eur Ceram Soc* 2004;**24**:825–31.
26. Reynaud C, Thévenot F, Chartier T, Besson JL. Mechanical properties and mechanical behaviour of SiC dense-porous laminates. *J Eur Ceram Soc* 2005;**25**:589–97.
27. Mistler RE, Twiname ER. *Tape casting. Theory and practice*. USA: The American Ceramic Society; 2000.
28. Boch P, Chartier T, Huttepain M. Tape casting of Al_2O_3/ZrO_2 laminated composites. *J Am Ceram Soc* 1986;**69**:191–2.
29. Tok AIY, Boey FTC, Khor KA. Tape casting of high dielectric ceramic composite substrates for microelectronic application. *J Mater Proc Technol* 1999;**89**(90):508–12.
30. Yuping Z, Dongliang J, Greil P. Tape casting of aqueous Al_2O_3 slurries. *J Eur Ceram Soc* 2000;**20**:1691–7.
31. Zhang GJ, Yue XM, Watanabe T. Al_2O_3/TiC/($MoSi_2 + Mo_2B_5$) multilayer composite prepared by tape casting. *J Eur Ceram Soc* 1999;**19**:2111–6.
32. Albano MP, Garrido LB. Influence of the slip composition on the properties of tape-cast alumina substrates. *Ceram Int* 2005;**31**:57–66.
33. Biamino S, Antonini A, Pavese M, Fino P, Badini C. $MoSi_2$ laminate processed by tape casting: microstructure and mechanical properties' investigation. *Intermetallics* 2008;**16**:758–68.
34. Biamino S, Liedtke V, Badini C, Euchberger G, Huertas Olivares I, Pavese M, et al. Multilayer SiC for thermal protection system of space vehicles: manufacturing and testing under simulated re-entry conditions. *J Eur Ceram Soc* 2008;**28**:2791–800.
35. Stavrinidis C, Tumino G, Caporicci M, Pradier A. European technology development efforts in the field of structures in preparation of future reusable space transportation systems. In: *Proceedings of the 1st AIAA/IAF Symposium on Future Reusable Launch Vehicles*. 2002. p. 1830.
36. Hass DD, Parrish PA, Wadley HNG. Electron beam directed vapor deposition of thermal barrier coatings. *J Vac Sci Technol, A* 1998;**16**: 3396–401.
37. Khor KA, Dong ZL, Gu YW. Plasma sprayed functionally graded thermal barrier coatings. *Mater Lett* 1999;**38**:437–44.
38. Badini C, Fino P, Ortona A, Amelio C. High temperature oxidation of multilayered SiC processed by tape casting and sintering. *J Eur Ceram Soc* 2002;**22**:2071–9.
39. Pavese M, Fino P, Ortona A, Badini C. Potential of SiC multilayer for high temperature applications in oxidising environment. *Ceram Int* 2008;**34**:197–203.
40. Specchia S, Civera A, Saracco G. In situ combustion synthesis of perovskite catalysts for efficient and clean methane premixed metal burners. *Chem Eng Sci* 2004;**59**:5091–8.
41. Biamino S, Fino P, Fino D, Russo N, Badini C. Catalyzed traps for diesel soot abatement: in situ processing and deposition of perovskite catalyst. *Appl Catal B* 2005;**61**:297–305.
42. Parker WJ, Jenkins RJ, Butler CP, Abbott GL. Flash method of determining thermal diffusivity, heat capacity, and thermal conductivity. *J Appl Phys* 1961;**32**:1679–84.
43. Lewis JA. Binder removal from ceramics. *Annu Rev Mater Sci* 1997;**27**:147–73.
44. Stobierski L, Gubernat A. Sintering of silicon carbide. I. Effect of carbon. *Ceram Int* 2003;**29**:287–92.